FASJS

Faculty of Arts and Science Journal of Science

SÜLEYMAN DEMİREL ÜNİVERSİTESİ

SÜLEYMAN DEMİREL
ÜNİVERSİTY

Süleyman Demirel University
Faculty of Arts and Sciences
Journal of Science

Volume

18

Issue

1

Year

2023

e-ISSN

1306-7575

Journal Boards

Süleyman Demirel University Faculty of Arts and Science Journal of Science is a peer-reviewed scientific journal published semi-annually, in May and November.

Original scientific research articles submitted in English in the fields of Biology, Physics, Chemistry and Mathematics are continued in the scientific review process after the preliminary evaluation stage, where similarity and layout checks are made.

No fee is charged from the author or institution under any name.

Special numbers/issues can be published without changing the periodic publication frequency during the year.

Since 2017; technical notes, letters to the editor, discussions, case reports and reviews will not be accepted.

As of 01.01.2023, Süleyman Demirel University Faculty of Arts and Sciences Journal of Science will only accept studies submitted in English.

Süleyman Demirel University Faculty of Arts and Science Journal of Science (SDUFASJS) takes into account the principles published by the Higher Education Institutions Scientific Research and Publication Ethics Directive and "Committee on Publication Ethics" (COPE). In this context, the issues that are important for the authors, referees and editors are specified in the "Ethical Principles and Publication Policy" page of the journal website.

Süleyman Demirel University Faculty of Arts and Science Journal of Science is indexed in the following databases.

- ULAKBIM TR – Dizin
- Bielefeld Academic Search Engine (BASE)
- Centre for Agriculture and Bioscience International (CABI) - CAB Direct
- China National Knowledge Infrastructure (CNKI)
- Crossref
- Directory of Open Access Journals (DOAJ)
- Directory of Open Access Scholarly Resources (ROAD)
- EBSCO host
- Elektronische Zeitschriftenbibliothek (EZB)
- German Union Catalogue of Serials (ZDB)
- Google Academic
- Index Copernicus
- Information Matrix for the Analysis of Journals (MIAR)
- MathSciNet
- ResearchBib
- WorldCat

Süleyman Demirel Üniversitesi Fen Edebiyat Fakültesi Fen Dergisi https://dergipark.org.tr/sdufeffd
Süleyman Demirel University Faculty of Arts and Sciences Journal of Science e-ISSN: 1306-7575
Volume: 18, Issue: 1, Year: 2023

CONTENTS

Süleyman Demirel Üniversitesi Fen Edebiyat Fakültesi Fen Dergisi https://dergipark.org.tr/sdufeffd
Süleyman Demirel University Faculty of Arts and Sciences Journal of Science e-ISSN: 1306-7575
Research Article, 2023, 18(1): 1-9, DOI: 10.29233/sdufeffd.1241050

Evaluation of X-Ray Shielding Ability of Tungsten Rubber: A GAMOS Monte Carlo Study

Meryem Cansu Şahin[1,*], Kaan Manisa[2]

[1]Department of Medical Services and Techniques, Vocational School of Health Services, Usak University, 64000, Usak, TURKEY
https://orcid.org/0000-0002-5743-3734
*corresponding author: meryem.sahin@usak.edu.tr
[2]Department of Physics, Faculty of Science and Arts, Kutahya Dumlupınar University, 43000, Kutahya, TURKEY
https://orcid.org/ 0000-0002-4063-277X

(Received: 23.01.2023, Accepted: 10.04.2023, Published: 25.05.2023)

Abstract: Against the detrimental effects of ionizing radiation, time, distance, and shielding are the three most significant protective methods. Lead is the material of choice for shielding, particularly for personal protective equipment. However, lead's density, rigidity, and toxicity are significant disadvantages. In recent years, tungsten-containing rubber (TCR) and other lightweight, flexible, and non-toxic shielding materials have emerged as viable alternatives to lead. The purpose of this study is to examine the X-ray absorption capacity of TCR material, which can serve as an alternative to lead-based personal protective equipment. Using GAMOS simulation, radiation absorption characteristics for 11 different X-ray energies ranging from 30 to 1000 keV were obtained and compared with Phy-X/PSD data. While the MFP value produced from the GAMOS code for the TCR with 100 keV energy X rays was 0.0204 cm, the Phy-X/PSD value was 0.0296 cm. The HVL value of the TCR material for X-rays with an energy of 100 keV was 0.021 cm for Phy-X/PSD and 0.014 cm for GAMOS. It has been observed to provide excellent radiation protection against X-rays in the diagnostic imaging field. By providing greater flexibility than lead shielding materials, TCR can play a crucial role in decreasing radiation exposure.

Key words: GAMOS, Phy-X PSD, Shielding

1. Introduction

Numerous radiation workers and patients are exposed to the adverse consequences of ionizing radiation, particularly in interventional radiology [1]. As a result of the stochastic effects of radiation [2], radiation workers are exposed to considerable dangers such as cancer incidence and cataracts. Thanks to adequate shooting methods and the capabilities of imaging technologies, measures are taken to limit patients' exposure to radiation. Nevertheless, personal protective equipment is the most effective method for protecting radiation workers from the damaging effects of ionizing radiation [3]. Lead is the preferred material for manufacturing this equipment. In spite of the fact that lead aprons are good at shielding X-rays, they have a variety of disadvantages for everyday use. The first of these is the equipment's weight. It has been noted that regular use of heavy personal protection equipment causes back pain or disc disease [4, 5]. In addition, lead, which has very little flexibility, can cause movement restrictions during the process. The radiation absorption capability of this personal protective equipment degrades with time as a result of use-related cracking. Another drawback is that lead is toxic to the human body and has negative environmental impacts [6–8].

The Tungsten-containing rubber (TCR) produced by Hayakawa Rubber Co., Ltd. (Hiroshima, Japan) is 0.5 mm thick and includes 90% tungsten powder by mass. TCR element ratios (mol%) are as follows: 1.0% hydrogen, 6.5% carbon, 0.5% oxygen, and 90.0% tungsten [9]. As indicated in Table 1 [10], the dry mass, thickness, tensile strength, wet strength, rip strength, and air resistance of the TCR were in accordance with the Japanese Industrial Standards for paper manufacturing. The TCR was determined to be a weak material in water, with a tensile strength of 118 N/15 mm in dry conditions and 5.9 N/15 mm in wet conditions. With a thickness of 5.23 mm, the TCR was similar to 3.32 mm of lead [11].

Table 1. The physical properties of TCR: The techniques of measurement for each property are provided in the columns to the right [11].

Bone-dry basis weight ($g.m^{-2}$)	700	JIS-P8124
Thickness (mm)	0.3	JIS-P8119
Tensile strength (N/15 mm)	118	JIS-P8113
Wet strength (N/15 mm)	5.9	JIS-P8135
Tear strength (mN)	220	JIS-P8116

The purpose of this study is to examine the TCR's ability to absorb x-rays using a GAMOS code. With the Architecture for Medicine-Oriented Simulations (GAMOS) code, the linear attenuation coefficient (μ), mass attenuation coefficient (μ_m), half value layer (HVL), tenth value layer (TVL), and mean free path (MFP) of TCR were computed. GAMOS simulation data for TCR was compared with Phy-X/PSD software data.

2. Material and Method

GAMOS v.6.2.0 software program was used for the simulations in this study. GAMOS is based on GEANT4 and is widely used for simulation studies in medical physics [12-13]. 400 cm away from the radiation source, a 50x50x2 mm^3 polyvinyltoluene (PVT) plastic scintillator was defined in the geometry file. The PMT on the top center of the PVT was assumed to be 50 mm in diameter and 100 mm tall. At the middle between the detector and the radiation source, TCR shielding material of 100 × 100 x 5 mm^3 was positioned (Figure 1).

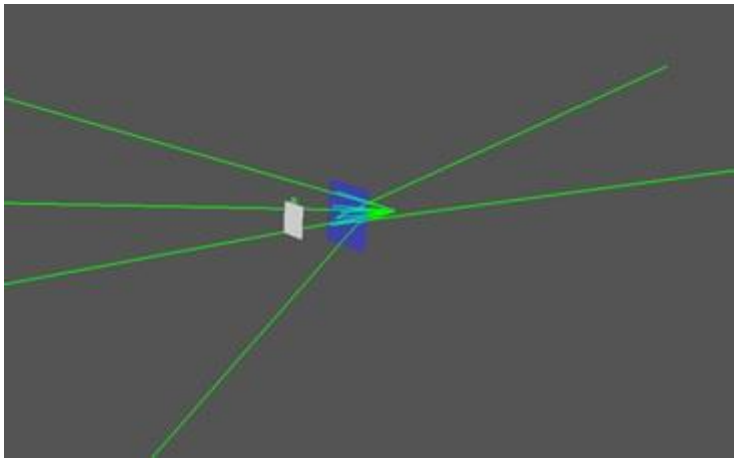

Figure 1. Simulation geometry.

In the input file, the physics, generator, and dose collection parameters were defined. In the simulation, the electromagnetic physics package was utilized. As radiation sources, gamma photons with energy of 30, 50, 60, 80, 100, 200, 300, 400, 500, 600, and 1000 keV were utilized, respectively. For scoring criteria, the amount of dose that reached the

detector via "dose deposit" was tallied. Although all physics processes were included into the scoring, variance reduction techniques were not implemented. Photon intensity values obtained with and without TCR in the simulation will be obtained as transmitted (I) and primary (I_0) intensities, respectively. A history of 10^7 photons was utilized, yielding sufficient results to improve the precision of the Monte Carlo simulations and reduce statistical error.

$$I = I_0 . e^{(-\mu . x)} \quad (1)$$

μ values at different energies were calculated for TCR using Beer Lambert's law (Eq. 1). As shown in Equation 2, μ_m is derived by dividing μ by the density (ρ) of the material.

$$Mass\ Attenuation\ Coefficient\ (\mu_m) = \mu/\rho \quad (2)$$

The MFP is defined as the average distance at which a radiation can be stopped in a material and is calculated using Equation 3.

$$Mean\ Free\ Path\ (MFP) = \mu^{-1} \quad (3)$$

HVL and TVL are the shield material thicknesses corresponding to the half and tenth values of the intensity of the incoming radiation, and they are given in Equations 4 and 5, respectively.

$$Half\ Value\ Layer\ (HVL) = \frac{ln2}{\mu} \quad (4)$$

$$Tenth\ Value\ Layer\ (TVL) = \frac{ln10}{\mu} \quad (5)$$

The physical properties of the TCR used in the GAMOS code were defined in the Phy-X/PSD [14] program and the μ, μ_m, HVL, TVL and MFP values were calculated. GAMOS simulation and Phy-X/PSD data were compared with each other.

3. Results and Discussion

There are various forms of radiation, including neutrons, X-rays, gamma rays, and so on. Different lead alloys and composites are used in the commercial market as gamma radiation shielding materials. High lead content, however, prevents its widespread use [15-17]. Tungsten, on the other hand, is a great gamma-ray shield because it is non-toxic and has a large gamma-ray scattering cross-section [18-19]. There is a current market demand for gamma-ray shielding items that are flexible, have a high gamma-ray shielding ability, and have precise mechanical properties [20].

In this study, the ability of TCR to shield X-rays of different energies was investigated by GAMOS simulation. The GAMOS simulation was used to get the TCR's radiation absorption parameters (μ, μ_m, MFP, HVL, and TVL) for 11 different X-ray energies ranging from 30 to 1000 keV (Table 2).

Table 2. The μ, μ_m and, MFP values of TCR at different energies.

Energy (keV)	μ (cm^{-1})		μ_m (cm^2/g)		MFP (cm)	
	Phy-X/PSD	GAMOS	Phy-X/PSD	GAMOS	Phy-X/PSD	GAMOS
30	172.976	169.830	22.611	22.346	0.0058	0.0059
50	81.198	77.316	5.920	5.918	0.0221	0.0358
60	28.260	27.897	3.694	3.671	0.0354	0.0222
80	59.432	64.008	7.769	8.685	0.0168	0.0151
100	33.771	40.951	4.414	5.441	0.0296	0.0204
200	5.975	9.270	0.781	1.220	0.1674	0.1079
300	2.469	3.212	0.323	0.423	0.4051	0.3113
400	1.469	1.247	0.192	0.164	0.6809	0.8019
500	1.052	0.790	0.138	0.104	0.9504	1.0659
600	0.835	0.559	0.109	0.074	1.1976	1.3882
1000	0.506	0.042	0.066	0.005	1.9756	2.0964

These parameters were then compared with the data from the Phy-X/PSD program. The geometry presented in Figure 1 was used to calculate the radiation absorption properties of the materials.

It is seen in Figure 2 that the μ value decreases as the photon energy increases. A peak between 80 and 90 keV was observed for the μ value. The μ value for 60 keV X-rays was 28.260 and 27.897 cm^{-1} for Phy-X/PSD, and GAMOS, respectively.

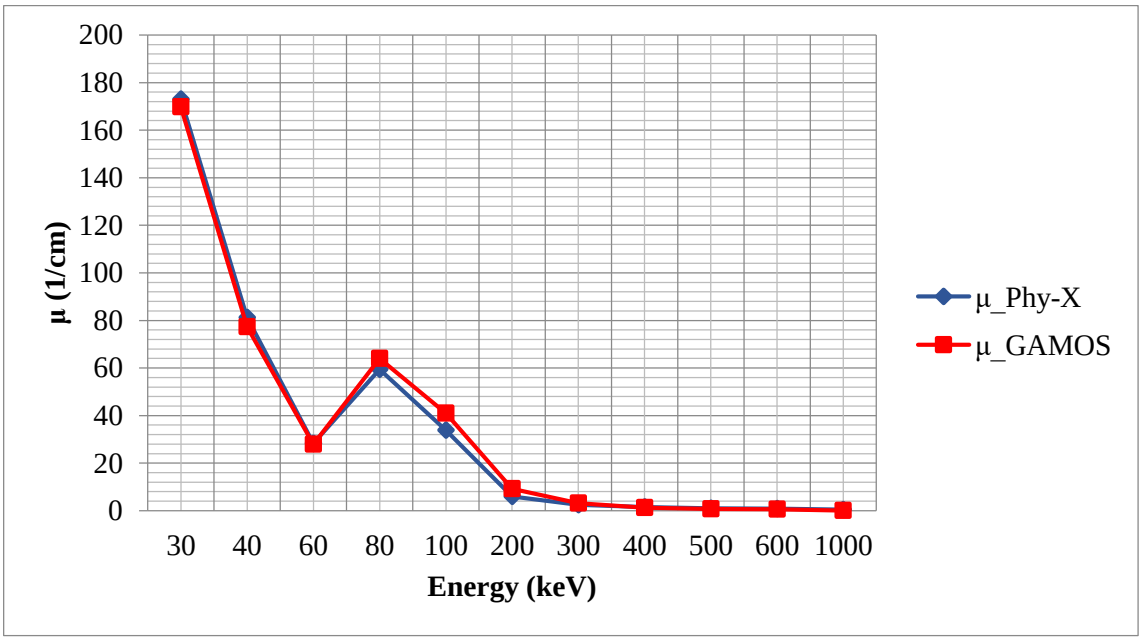

Figure 2. The μ values of TCR at different energies

The μ_m value decreased as the photon energy increased (Figure 3). The μ_m value for X-rays with 400 keV energy was 0.192 and 0.164 g/cm^2 for Phy-X/PSD, and GAMOS, respectively. As expected, maximum μ and μ_m values were observed at lower photon energies due to photoelectric interactions between photons and TCR atoms with high atomic numbers. Later, as the probability of photon penetration increased with the increased photon energy, these values rapidly decreased. On the other hand, the more photon energy increased, the Compton scattering effect was overwhelmed, and the weakening of TCR atoms was more dependent on the electron density than the atomic number. Therefore, TCR's mass attenuation coefficients have decreased with increased gamma-ray energies.

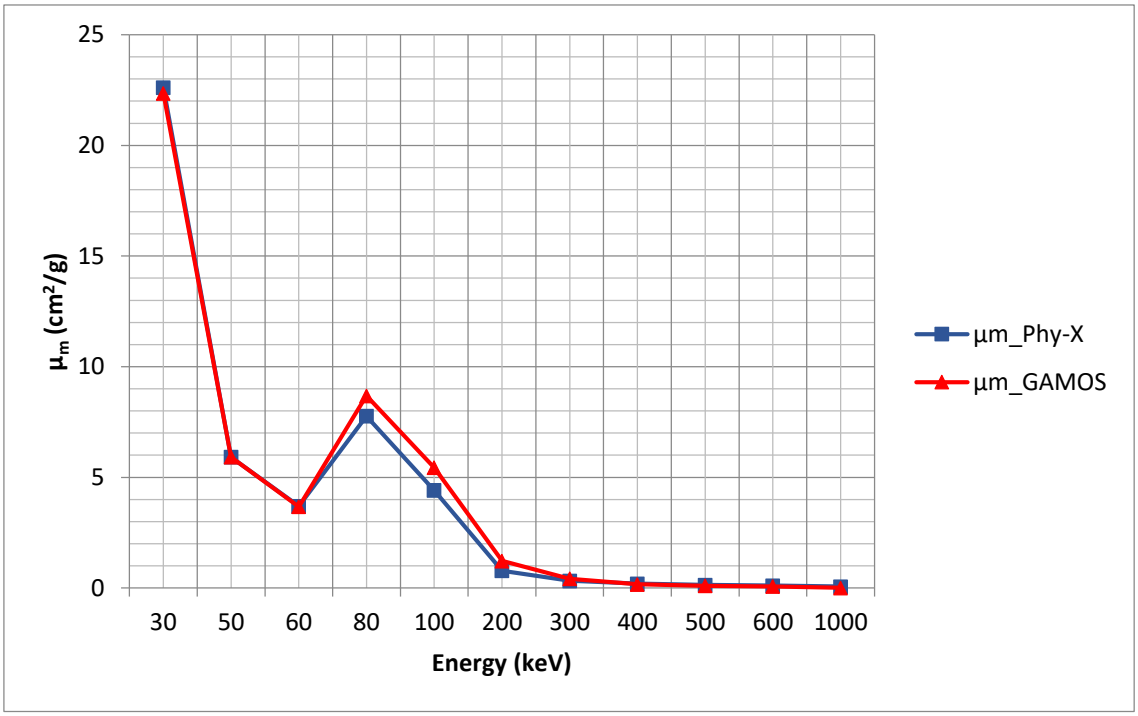

Figure 3. The μ_m values of TCR at different energies

MFP values obtained using both GAMOS and Phy-X/PSD were directly proportional to energy (Figure 4). The MFP value obtained from the GAMOS code for TCR with 100 keV energy X-rays was 0.0204 cm, while this value was 0.0296 cm for Phy-X/PSD.

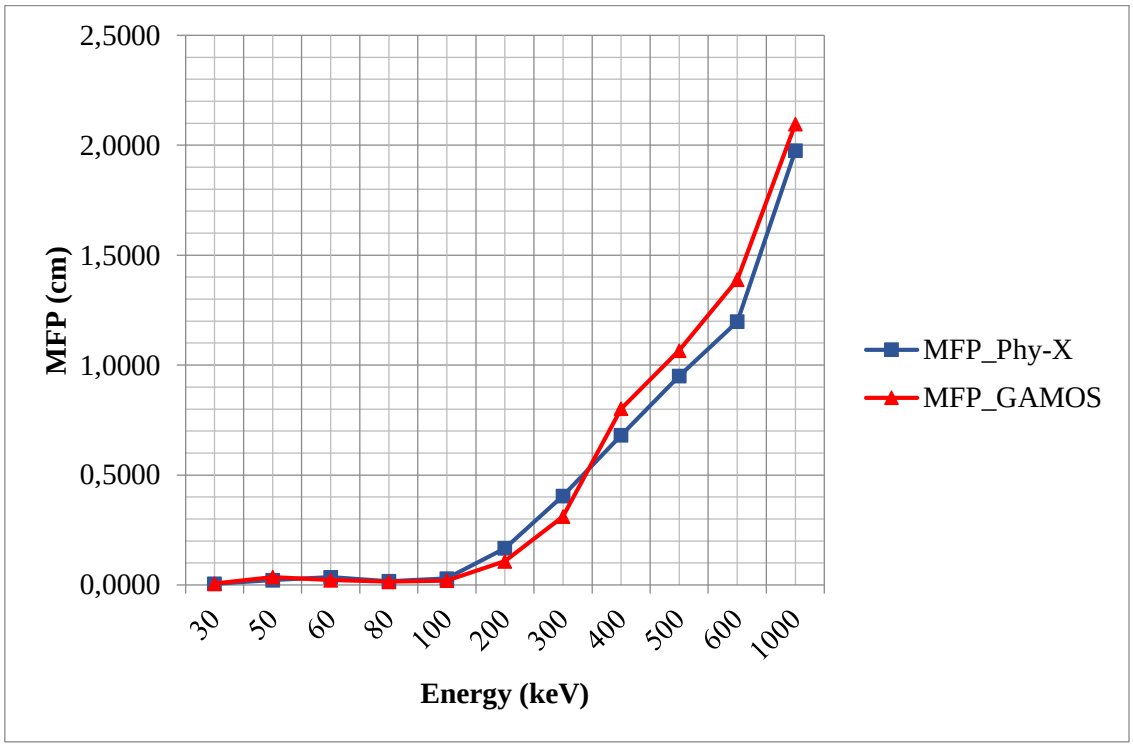

Figure 4. The MFP values of TCR at different energies

Xu et al. [21] found that the radiation absorption rates of tungsten-doped rubber composites of 5 and 6 mm thickness at 0.667 MeV gamma-ray energy were 20.6% and 25%, respectively. The gamma ray shielding rate of tungsten-doped rubber composites with a thickness of 10 mm is around 45.2%, demonstrating excellent gamma ray shielding performance [10].

The μ values of hybrid elastomers doped with tungsten in various proportions ranges from 0.078 cm^{-1} for pure polymer (0% tungsten) to 0.688 cm^{-1} for 88.1% tungsten. Gamma rays with a wavelength of 0.662 MeV can be attenuated by 49.74% by a 1 cm thick shielding material containing 88.1% tungsten by weight. In the same study, the μ_m increases from 0.0789 cm^2/g at 0% wt to 0.1035 cm^2/g at 88.1% wt [20]. Despite the fact that the mass attenuation coefficient of pure tungsten is 0.0933 cm^2/g [22], the TCR has a greater value due to the lower density. In addition to possessing outstanding shielding qualities, TCR also possesses elastomer-like properties. In our study, μ values obtained from GAMOS simulation for TCR ranged from 0.042 to 169.830 cm^{-1}. μ values were between 0.506 and 172.976 cm^{-1} in the Phy-X/PSD program. The μ_m values ranged between 0.005 and 22.346 cm^2/g according to the GAMOS code. The μ_m values obtained for TCR from the Phy-X/PSD program were between 0.066 and 22.611 cm^2/g and were consistent with the GAMOS results (Figure 2). As expected, the values of μ and μ_m decreased with the increase in incident photon energies. At lower energies, where photoelectric absorption predominates, the μ_m values have maximum values [24]. However, it has been demonstrated that TCR effectively absorbs photons and reduces transmitted radiation. At medium and higher energies, however, the contribution of Compton scattering is not negligible relative to photoelectric absorption. Therefore, different ratios of the same material by weight cause a change in the mass attenuation coefficient.

For the TCR, the HVL values calculated with the data obtained from GAMOS in the energy range of 30–1000 keV varied between 0.004–1.470 cm (Figure 5). The HVL value of the TCR material for X-rays with 100 keV energy was 0.021 and 0.014 cm for Phy-X/PSD, and GAMOS, respectively (Table 3). In the 30-1000 keV energy range, the TVL values calculated from the GAMOS code varied between 0.014 and 5.048 cm (Figure 5) (Table 3).

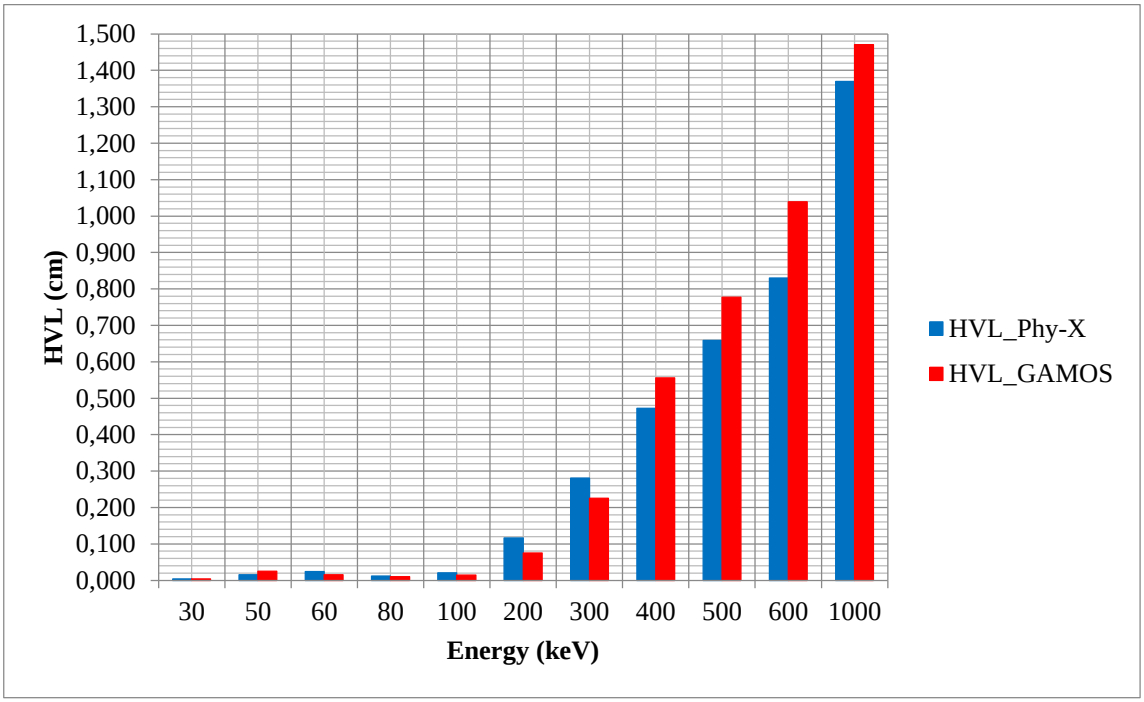

Figure 5. HVL values of TCR at different energies.

Table 3. HVL and TVL values of TCR at different energies.

Energy (keV)	HVL (cm)		TVL (cm)	
	Phy-X/PSD	GAMOS	Phy-X/PSD	GAMOS
30	0.004	0.004	0.013	0.014
50	0.015	0.025	0.051	0.051
60	0.025	0.015	0.081	0.083
80	0.012	0.011	0.039	0.035
100	0.021	0.014	0.068	0.047
200	0.116	0.075	0.385	0.248
300	0.281	0.226	0.933	0.717
400	0.472	0.556	1.568	1.846
500	0.659	0.777	2.188	2.515
600	0.830	1.040	2.757	2.518
1000	1.369	1.470	4.549	5.048

Other parameters to compare the shielding efficiency of a material are its HVL and TVL. HVL decreases from 8.88 to 1.01 cm with a change in weight percent of tungsten from 0% to 88.1%. At 662 keV energy, the HVL of 88.1 wt% tungsten-loaded composites is 1.01 cm [20]. Tungsten-lead wool blankets (T-Flex® W, 88% W by mass) suspended in polymer are another material used for radiation shielding. At 662 keV, the HVL for T-Flex® W is 2.2 cm [24]. In our study, the TCR's $HVL_{Phy\text{-}X}$ and HVL_{GAMOS} values for X-rays with 600 keV energies were found to be 0.830 and 1.040 cm, respectively. At higher photon energies, HVL and TVL values increased. The exchange of HVL and TVL at different photon energies can be confirmed based on the dominance of various photon interactions in different energy regions. In addition, the HVL values increased at higher photon energies, and the HVL variation with the photon energy in these samples could be justified based on the dominance of various photon interaction processes in different energy regions, as discussed above in the mass attenuation coefficients. Notably, lower HVL values were required for a better gamma-ray shielding material as it provided a higher probability of photon interactions with the material.

4. Conclusion

TCR is a new flexible protective material that contains a metal with a high atomic number in rubber and has a shielding ability equivalent to or higher than lead. It has been observed to provide excellent radiation protection against X-rays in the diagnostic imaging field. It can help reduce radiation exposure in a big way because it is more flexible than lead shielding materials.

Authorship contribution statement

M. C. Şahin: Conceptualization, Methodology, Data Curation, Original Draft Writing; **K. Manisa**: Conceptualization, Methodology, Visualization, Supervision/Advice.

Declaration of competing interest

The authors declare that they have no known competing financial interests or personal relationships that could have appeared to influence the work reported in this paper.

Ethics Committee Approval and/or Informed Consent Information

As the authors of this study, we declare that we do not have any ethics committee approval and/or informed consent statement.

References

[1] T. B. Shope, "Radiation-induced skin injuries from fluoroscopy", *Radiographics*, 16(5), 1195-1199, 1996.

[2] H. Monzen, M. Tamura, K. Shimomura, Y. Onishi , S. Nakayama, T. Fujimoto, K. Matsumoto, K. Hanaoka and T. Kamomae, "A novel radiation protection device based on tungsten functional paper for application in interventional radiology", *Journal of Applied Clinical Medical Physics*, 18(3), 215-220, 2017.

[3] K. Chida, Y. Morishima, Y. Katahira, H. Chiba and M. Zuguchi, "Evaluation of additional lead shielding in protecting the physician from radiation during cardiac interventional procedures", *Nihon Hoshasen Gijutsu Gakkai Zasshi*, 61(12), 1632-1637, 2005.

[4] R. Jiang, M. Chen, Q. Liu, G. Fu, Y.Xue, H. Fu, S. Wu, C. Ma, D. Long and C. Jiang, "Body pain - An unheeded personal health hazard in interventional cardiologists: A national online cross-sectional survey study in China", *International Journal of Cardiology*, 350, 27-32, 2022.

[5] S. Andrew, M. R Abdelmonem, S. Kohli and H. Dabke, "Evaluation of Back pain and Lead apron use among staff at a district general hospital", *Cureus*, 13(10), 2021.

[6] P. B. Tchounwou, C. G. Yedjou, A. K. Patlolla and D. J. Sutton, "Heavy metal toxicity and the environment", *Experientia Supplementum*, 101(2012), 133-164, 2012.

[7] A. M.Scheuhammer and S. L. Norris, "The ecotoxicology of lead shot and lead fishing weights", *Ecotoxicology*, 5(5), 279-295, 1996.

[8] N. Moonkum, C. Pilapong, K. Daowtak and G. Tochaikul, "Evaluation of silicone rubber shielding material composites enriched with BaSO4 and Bi2O3 particles for radiation shielding properties", *Materials Research Innovations*, 1-8, 2022.

[9] K. Kijima, H. Monzen, K. Matsumoto, M. Tamura and Y. Nishimura, "The shielding ability of novel tungsten rubber against the electron beam for clinical use in radiation therapy", *Anticancer Research*, 38(7), 3919-3927, 2018.

[10] H. Monzen, I. Kanno, T. Fujimoto and M. Hiraoka, "Estimation of the shielding ability of a tungsten functional paper for diagnostic x-rays and gamma rays", *Journal of Applied Clinical Medical Physics*, 18(5), 325-329, 2017.

[11] H. Kosaka, H. Monzen, K. Matsumoto, M. Tamura and Y. Nishimura, "Reduction of Operator Hand Exposure in Interventional Radiology With a Novel Finger Sack Using Tungsten-containing Rubber", *Health Physics*, 116(5), 625-630, 2019.

[12] P. Arce, S. Banerjee, TBoccali, M. Case, A. D. Roeck, V. Lara, M. Liendl, A. Nikitenko, M. Schroder, A. Straessner, H. P. Wellisch and H. Wenzel, "Simulation framework and XML detector description for the CMS experiment", *Nuclear Instruments and Methods in Physics Research Section A: Accelerators, Spectrometers, Detectors and Associated Equipment*, 502(2), 687-688, 2003.

[13] P. Arce, I. J. Lagares, L. Harkness, D. P. Astudillo, M. Cañadas, P. Rato, M. D. Prado, Y. Abreu, G. Lorenzo, M. Kolstein and A. Díaz, "Gamos: A framework to do Geant4 simulations in different physics fields with an user-friendly interface", *Nuclear Instruments and Methods in Physics Research Section A: Accelerators, Spectrometers, Detectors and Associated Equipment*, 735, 304-313, 2014.

[14] E. Şakar, Ö. F. Özpolat, B. Alim, M. Sayyed and M. Kurudirek, "Phy-X / PSD: Development of a user friendly online software for calculation of parameters relevant to radiation shielding and dosimetry", *Radiation Physics and Chemistry*, 166(2020), 1-12, 2020.

[15] S. Chambial, P. Bhardwaj, A. A. Mahdi and P. Sharma, "Lead poisoning due to herbal medications", *Indian Journal of Clinical Biochemistry*, 32(2), 246-247, 2017.

[16] Y. Li, H. Lv, C. Xue, N. Dong, C. Bi and A. Shan, "Plant polyphenols: Potential antidotes for lead exposure", *Biological Trace Element Research*, 199(10), 3960-3976, 2021.

[17] A. L. Wani, A. Ara and J. A. Usmani, "Lead toxicity: a review", *Interdisciplinary Toxicology*, 8(2), 55-64, 2015.

[18] B. Zeng, W. Huang, X. Zeng, J. Hu, Y. Hu and T. Zhang, "Adsorption properties and kinetic of WD918 ion exchange resin for molybdenum from ammonium tungstate solutions", *Sustainability*, 44(7), 1-14, 2020.

[19] P. Atashi, S. Rahmani, B. Ahadi and A. Rahmati, "Efficient, flexible and lead-free composite based on room temperature vulcanizing silicone rubber/W/Bi2O3 for gamma ray shielding application", *Journal of Materials Science: Materials in Electronics*, 29(14), 12306-12322, 2018.

[20] B. Ahmed, G. Shah, A. H. Malik and M. Rizwan, "Gamma-ray shielding characteristics of flexible silicone tungsten composites", *Applied Radiation and Isotopes*, 155,1-7, 2020.

[21] X. R. Xu, J. Q. Wu, J. Xu, F. Liu, A. Xie, J. L. Liu and M. Zhang, "Preparation of flexible rubber composites with high contents of tungsten powders for gamma radiation shielding", *Rare Metals*, 41(7), 2243-2248, 2022.

[22] J. R. Lamarsh and A. J. Baratta, Introduction to Nuclear Engineering, New Jersey, Prentice Hall Upper Saddle River, 801 pages, 2001.
[23] V. S. Zali, O. Jahanbakhsh and I. Ahadzadeh, "Preparation and evaluation of gamma shielding properties of silicon-based composites doped with WO3 micro- and nanoparticles", *Radiation Physics and Chemistry*, 197(2022), 1-10, 2022.
[24] D. R. McAlister, "Gamma ray attenuation properties of common shielding materials", Ph.D. thesis, University Lane Lisle, IL, USA, 2018.

Süleyman Demirel Üniversitesi Fen Edebiyat Fakültesi Fen Dergisi https://dergipark.org.tr/sdufeffd
Süleyman Demirel University Faculty of Arts and Sciences Journal of Science e-ISSN: 1306-7575
Research Article, 2023, 18(1): 10-17, DOI: 10.29233/sdufeffd.1244542

Validation of a Proposed Equation for Determining the Half-Thickness Value of Gamma and X-Ray Radiation

Meryem Cansu Şahin[1,*], Kaan Manisa[2], Hasan Bircan[3]

[1]Department of Medical Services and Techniques, Vocational School of Health Services, Usak University, 64000, Usak, TURKEY
https://orcid.org/0000-0002-5743-3734
*corresponding author: meryem.sahin@usak.edu.tr
[2]Department of Physics, Faculty of Science and Arts, Kutahya Dumlupınar University, 43000, Kutahya, TURKEY
https://orcid.org/ 0000-0002-4063-277X
[3]Department of Physics, Faculty of Science and Arts, Kutahya Dumlupınar University, 43000, Kutahya, TURKEY
https://orcid.org/ 0000-0003-2067-7855
(Received: 30.01.2023, Accepted: 17.04.2023, Published: 25.05.2023)

Abstract: Half-value layer (HVL) is energy dependent on the photon, much as the attenuation coefficient. Increasing the penetrating energy of a photon stream causes an increase in a substance's HVL. Before calculating the HVL value, the linear attenuation coefficient (μ) must be established. A review of the literature indicated that there is presently no Monte Carlo-based sufficient tool for direct calculation of the HVL value and direct computation suitable for material design and all changes based on sophisticated simulation methods. This study aims to calculate HVL data with GAMOS simulation in the 0.1-20 MeV energy range for some anatomical structures defined in ICRU-44 (bone cortical, brain, gray/white matter, breast tissue, eye lens, and testis). The HVL values of the anatomical structures used in the GAMOS code were compared with the results in the literature. As a result, HVL values obtained from GAMOS simulation for different materials and biological structures were compatible with the literature.

Key words: GAMOS, Half-Value Layer, Radiation.

1. Introduction

X and gamma photons, commonly utilized for medical diagnosis and therapy, belong to the class of ionizing radiation. When photons transfer some of their energy to electrons in the medium, ionization and excitation occur, increasing the risk of future stochastic and deterministic effects in biological systems [1]. Deterministic or stochastic effects of radiation in biological environments are tried to be understood by using linear (μ) or mass (μ/ρ) energy absorption coefficients. Both quantities show how likely it is that one photon per unit mass of the absorbing medium will scatter or be absorbed or how likely it is that energy will be taken in [2]. Absorption coefficient calculations can be made with software such as FLUKA, GEANT, and MCNP based on the Monte Carlo technique [3-5]. Estimating the absorption coefficient can be approximated using weight ratios for biological tissues and chemical mixtures [6]. GAMOS is based on GEANT4 and is widely used for simulation studies in medical physics [7, 8]. It has not yet been possible to derive the radiation absorption parameters of materials (Half-value layer (HVL), tenth-value layer (TVL), mean free path (MFP), etc.) from a generic formula.

HVL is one of the key characteristics associated with ionizing radiation [9, 10]. HVL refers to the material thickness necessary to reduce the air kerma intensity of the photon to half of its starting value. It is related to the material's linear attenuation coefficient

and photon energy. As opposed to linear and mass attenuation coefficients, which measure single energy rays, this coefficient is used to quantify polyenergetic rays [11]. The thickness of any substance in which fifty percent of incoming energy is absorbed is known as the HVL. Despite being a metric unit, HVL depends on energy and μ values. Increasing the penetrating energy of a photon beam causes the HVL of a substance to increase. The μ must be established before calculating the HVL value. HVL can be determined using μ, but there should be alternative, realistic ways independent of calculating the value of μ at any given energy level [12-14].

Bircan et al., in their article titled "A New Equation for Calculation of Gamma and X-ray Radiation Half Value Thickness", proposed an equation in which the half-value layer thickness can be directly calculated in the energy range of 0.001–20 MeV (Eq. 1) [15, 16].

$$Half\ Value\ Layer\ (HVL) = \frac{(a + bE + cE^2 + dE^3 + eE^4 + fE^5)}{(1 + gE + hE^2 + iE^3 + jE^4 + kE^5)} \quad (1)$$

They reported that the constants of the equation are specific for the radiation-absorbing substance, and the variation of half-value thickness values with energy can be shown [15].

This study aims to calculate HVL data with GAMOS simulation in the 0.1-20 MeV energy range for some anatomical structures defined in ICRU-44 (bone cortical, brain, gray/white matter, breast tissue, eye lens, and testis). The HVL values from the GAMOS simulation were compared with those from Equation 1 [15] and the NIST database [17].

2. Materials and Methods

GAMOS v.6.2.0 software was used for the simulations in this study. The geometry of the simulation includes a point source, six different 10x10x1 cm^3 absorbing targets (anatomical structures) that are 50 cm away, and a 20x20x20 cm^3 detector that is 100 cm from the radiation source. To prevent photon interactions with materials outside the sample, all components of the to-be-collected geometry were enclosed in a vacuum cube (300x300x300 cm^3) (Figure 1).

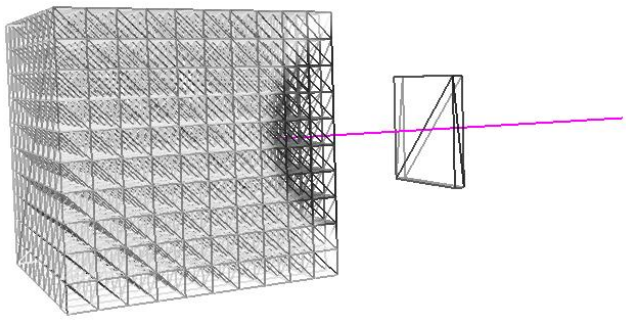

Figure 1. Simulation geometry.

The physics, generator, and dose collection parameters were defined in the input file. In the simulation, the electromagnetic physics package was utilized. The simulations were carried out at 9 different photon energies in the range of 0.1-20 MeV. The amount of dose that reached the detector via "dose deposit" was tallied for scoring criteria. Although all physics processes were included in the scoring, variance reduction techniques were not implemented. The I and I_0 values were acquired by repeatedly simulating the anatomical structures with and without shielding material. A history of 10^7 photons was utilized, yielding sufficient results to improve the precision of the Monte Carlo simulations and reduce statistical error.

$$I = I_0 . e^{(-\mu . x)} \tag{2}$$

μ values at different energies were calculated for anatomical structures using Beer Lambert's law (Eq. 2). As shown in Equation 2, μ/ρ is derived by dividing μ by the density (ρ) of the material (Eq. 3).

$$Mass\ Attenuation\ Coefficient\ = \mu/\rho \tag{3}$$

HVL is the shield material thickness corresponding to the half-values of the intensity of the incoming radiation, and they are given in Equation 4.

$$Half\ Value\ Layer\ (HVL) = \frac{ln2}{\mu} \tag{4}$$

HVL values of anatomical structures obtained from GAMOS simulation and Equation 1 were compared. The difference between the simulation and Equation 1 values of HVL was calculated using Equation 5.

$$Difference\ (\%) = \left|\frac{*\ HVL - HVL}{HVL}\right| X\ 100\% \tag{5}$$

In Equation 5, *HVL values were obtained by Equation 1, and HVL values were obtained by GAMOS simulation.

3. Results and Discussion

In this study, the amount of X-ray absorption of different anatomical structures was investigated by GAMOS simulation. The μ and HVL parameters of some anatomical structures in the ICRU-44 were obtained from GAMOS simulation for 9 different photon energies ranging from 0.1-20 MeV. These parameters were compared with the HVL data from Equation 1 [15].

Figure 2 presents the energy-dependent graph of μ values obtained by the GAMOS simulation. It is seen that the value of μ decreases as the photon energy increases in all anatomical structures. The μ/energy curves for the brain, breast tissue, eye lens, and testis, which have similar densities, gave close results as expected. Bone with a density of 1.92 g/cm^3 had a decreasing curve as energy increased, but μ values were higher than those of other anatomical structures (Figure 2).

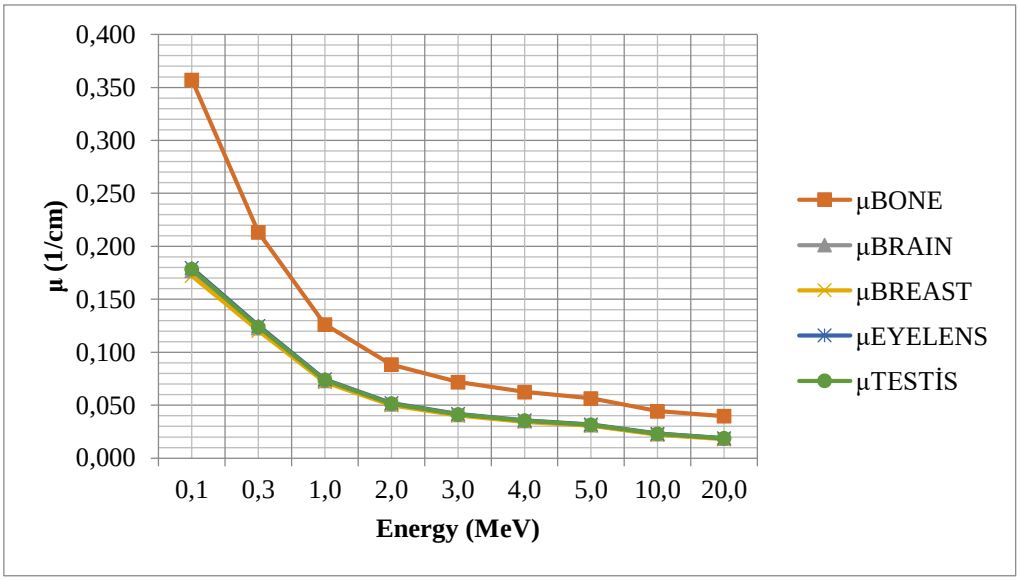

Figure 2. μ values of anatomical structures at different energies

The HVL values obtained with the GAMOS code of the anatomical structures and calculated with Equation 1 are shown in Table 1. HVL values obtained by both methods were compatible with each other. It has been verified by GAMOS simulation that Equation 1 can be used to quickly and reliably calculate the HVL value of a material.

Table 1. HVL values calculated using GAMOS, the NIST database and Equation 1.

Energy (MeV)	HVL_{BONE} (cm)			HVL_{BRAIN} (cm)			HVL_{BREAST} (cm)		
	**NIST	*Ref. Study	This Study	**NIST	*Ref. Study	This Study	**NIST	*Ref. Study	This Study
0.1	1.946	1.944	1.940	3.918	3.923	3.923	3.923	4.029	4.025
0.3	3.244	3.243	3.250	5.643	5.648	5.648	5.648	5.756	5.763
1.0	5.498	5.501	5.488	9.471	9.478	9.478	9.478	9.667	9.663
2.0	7.836	7.846	7.835	13.555	13.563	13.563	13.563	13.846	13.837
3.0	9.640	9.653	9.635	16.886	16.894	16.894	16.894	17.282	17.257
4.0	11.084	11.087	11.082	19.701	19.707	19.707	19.707	20.199	20.167
5.0	12.254	12.244	12.252	22.128	22.128	22.128	22.128	22.709	22.685
10.0	15.601	15.609	15.598	30.309	30.267	30.267	30.267	31.223	31.324
20.0	17.457	17.44	17.449	37.234	37.110	37.110	37.110	38.411	38.912

***** *Calculated with Equation 1 [15]* ****Calculated with NIST data [17].*

Table 1. HVL values calculated using GAMOS, NIST database and Equation 1. (continued)

Energy (MeV)	$HVL_{EYE\ LENS}$ (cm)			HVL_{TESTIS} (cm)		
	**NIST	*Ref. Study	This Study	**NIST	*Ref. Study	This Study
0.1	3.858	3.855	3.857	3.923	3.884	3.885
0.3	5.541	5.54	5.540	5.648	5.59	5.593
1.0	9.295	9.3	9.293	9.478	9.396	9.386
2.0	13.305	13.299	13.302	13.563	13.431	13.431
3.0	16.576	16.576	16.573	16.894	16.732	16.730
4.0	19.343	19.351	19.339	19.707	19.523	19.515
5.0	21.731	21.734	21.726	22.128	21.916	21.912
10.0	29.798	29.796	29.791	30.267	29.983	29.973
20.0	36.661	36.658	36.653	37.110	36.749	36.748

***** *Calculated with Equation 1 [15] ** Calculated with NIST data [17].*

The HVL values calculated by both methods increased as the photon energy increased for all anatomical structures. The HVL value for bone tissue of an x-ray photon with an energy of 0.1 MeV has been reported to be 1.94 cm [18]. Jarrah et al., in the study in which they compared the results obtained with the Monte Carlo simulation and the Geometric Progression fitting method, the HVL value for the breast tissue is approximately 30 cm [19]. Breast tissue was the anatomical structure with the highest HVL value in all photon energies. It was observed that the large photon attenuation effect of bone tissue made the HVL value lower than all other tissues examined.

The difference between the HVL values obtained by the two methods was below 2% for all anatomical structures (Table 2). For the breast, the difference between GAMOS at 20 MeV energy and the HVL value calculated with the formula suggested in the reference article is 1.3055% (Figure 3).

Table 2. Difference between HVL values obtained from GAMOS and reference article for each anatomical structure.

Energy (MeV)	Bone	Brain	Breast	Eye Lens	Testis
0.1	0.1900	0.1631	0.1005	0.0632	0.0164
0.3	0.2303	0.0493	0.1148	0.0058	0.0576
1.0	0.2298	0.0720	0.0405	0.0700	0.1100
2.0	0.1460	0.0213	0.0628	0.0209	0.0001
3.0	0.1847	0.0216	0.1441	0.0195	0.0117
4.0	0.0460	0.0665	0.1605	0.0619	0.0406
5.0	0.0636	0.0405	0.1063	0.0350	0.0167
10.0	0.0705	0.0124	0.3226	0.0157	0.0342
20.0	0.0520	0.0026	1.3055	0.0129	0.0018

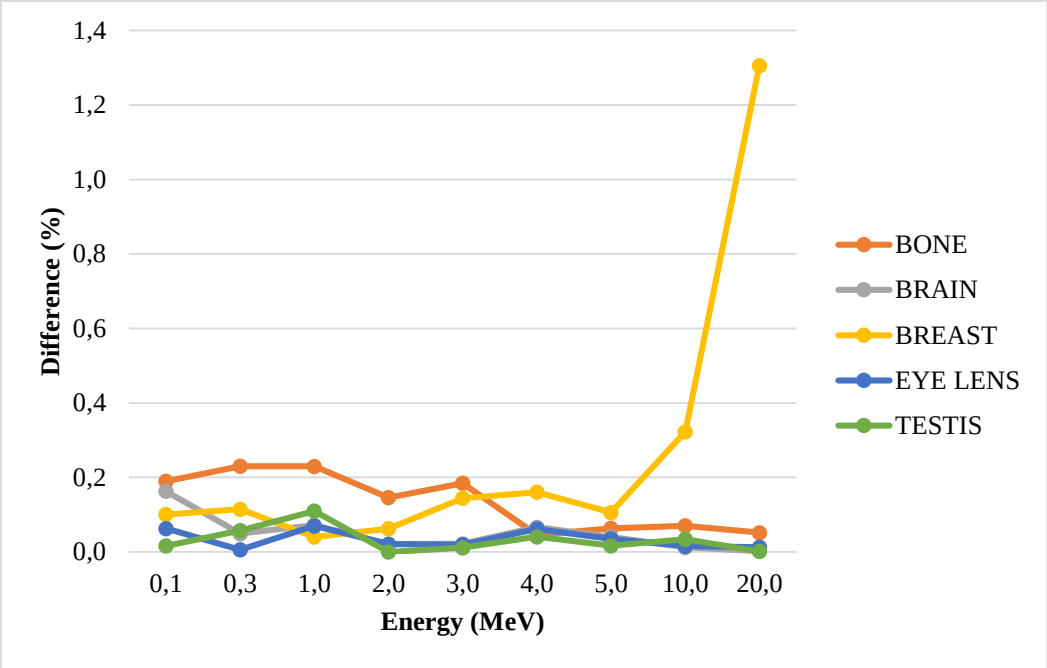

Figure 3. Difference between HVL values for each anatomical structure.

HVL is energy dependent on the photon, much as the attenuation coefficient. Increasing the penetrating energy of a photon stream causes an increase in a substance's HVL. The linear attenuation coefficient (μ) must be known before calculating the HVL value. While HVL can be computed using μ, alternative and practical techniques independent of the calculation of μ, the value at any energy level should be available [12-14]. The linear attenuation coefficient should be mainly obtained by experimental or theoretical approaches to compute the HVL. Since the linear attenuation coefficient is calculated for each energy value, the estimated HVL value will also include the half-value thickness at the relevant energy [20].

When reviewing the literature, it is discovered that innovative methodologies for computing HVL values are presented, which may give answers for medical and industrial radiation applications [9, 10, 18, 19]. A review of the literature indicated that there is presently no Monte Carlo-based sufficient tool for direct calculation of the HVL value and direct computation suitable for material design and all changes based on sophisticated simulation methods [9, 20]. The GAMOS code for all anatomical structures and the HVL data obtained with the formula suggested in the reference article were compatible.

4. Conclusion

In conclusion, the formula (Eq. 1) presented in the article "A New Equation for Calculation of Gamma and X-ray Radiation Half Value Thickness" agreed with the data from the GAMOS simulation. It was observed that the data obtained from the GAMOS simulation agreed with the findings obtained from both equation 1 presented in the reference article and the NIST database. Different radiation parameters can be formulated and brought to a level where they can be used, especially in medical physics.

Authorship Contribution Statement

M.C. Şahin: Conceptualization, Methodology, Data Curation, Original Draft Writing; **K. Manisa**: Visualization, Supervision/Advice; **H. Bircan:** Conceptualization, Methodology, Data Curation, Original Draft Writing.

Declaration of Competing Interest

The authors declare that they have no known competing financial interests or personal relationships that could have appeared to influence the work reported in this paper.

Ethics Committee Approval and/or Informed Consent Information

As the authors of this study, we declare that we do not have any ethics committee approval and/or informed consent statement.

References

[1] E. A. Domina and O. L. Kopylenko, "Role of radioprotectors in minimization of stochastic effects of radiation incidents", *Experimental Oncology*, 44(3), 186-189, 2022.

[2] J. K. Shultis and R. E. Faw, Fundamentals of Nuclear Science and Engineering, New York, Marcel Dekker Inc., 506 pages, 2002.

[3] T. Korkut, A. Karabulut, G. Budak and F. Demir, "Monte Carlo Simülasyonu ile Kolemanit Cevherinin Çeşitli Foton Enerjileri için Radyasyon Soğurganlığının Belirlenmesi," *X. Ulusal Nükleer Bilimler ve Teknolojileri Kongresi*, 6-9 Ekim, 2009, Muğla, s. 428–431.

[4] M. E. Medhat and V. P. Singh, "Mass attenuation coefficients of composite materials by Geant4, XCOM and experimental data: comparative study", *Radiation Effects & Defects in Solids*, 169(9), 800–807, 2014.

[5] P. Singh, A. M. Ali, N. M. Badiger and A. M. El-Khayatt, "Monte Carlo simulation of gamma ray shielding parameters of concretes", *Nuclear Engineering and Design*, 265, 1071–1077, 2013.

[6] National Institute of Standards and Technology Database, NIST. [Online]. Available: http://physics.nist.gov/xaamdi, Accessed: 21.02.2023.

[7] P. Arce, S. Banerjee, T. Boccali, M. Case, A. Roeck, V. Lara, M. Liendl, A. Nikitenko, M. Schroder, A. Straessner, H. P. Wellisch and H. Wenzel, "Simulation framework and XML detector description for the CMS experiment", *Nuclear Instruments and Methods in Physics Research Section A: Accelerators, Spectrometers, Detectors and Associated Equipment*, 502(2), 687-688, 2003.

[8] P. Arce, I. J. Lagares, L. Harkness, D. P. Astudillo, M. Cañadas, P. Rato, M. Prado, Y. Abreu, G. Lorenzo, M. Kolstein and A. Díaz, "Gamos: A framework to do Geant4 simulations in different physics fields with an user-friendly interface", *Nuclear Instruments and Methods in Physics Research Section A: Accelerators, Spectrometers, Detectors and Associated Equipment*,735,304-313, 2014.

[9] K. Matsubara, H. Nagata, R. Okubo, T. Takata and M. Kobayashi, ''Method for determining the half-value layer in computed tomography scans using a real-time dosimeter: application to dual-source dual-energy acquisition'', *Physica Medica*, 44(2017), 227-231, 2017.

[10] T. Gotanda, T. Katsuda, R. Gotanda, A. Tabuchi, K. Yamamoto, T. Kuwano, H. Yatake, K. Kashiyama and Y. Takeda, ''Half-value layer measurement: simple process method using radiochromic film'', *Australasian Physics & Engineering Sciences in Medicine*, 32(2009), 150-158, 2009.

[11] A. Fukuda, I. Nao, T. Masami, Y. Tensho, M. Katsuhiko and K. Hitoshi, ''Measurement of the half-value layer for CT systems in a single-rotation technique: Reduction of stray radiation with lead apertures'', *Physica Medica: European Journal of Medical Physics*, 76, 221 – 226, 2020.

[12] H.O. Tekin, F.T. Ali, G. Almisned, G. Susoy, S.A.M. Issa, A. Ene, W. Elshami and H.M.H. Zakaly, ''Multiple assessments on the gamma-ray protection properties of niobium-doped borotellurite glasses: a wide range investigation using Monte Carlo simulations'', *Science And Technology Of Nuclear Installation*, 2022, 1-17, 2022.

[13] H. M. H. Zakaly, Y. S. Rammah, H. O. Tekin, A. Ene, A. Badawi and S. A. M. Issa, ''Nuclear shielding performances of borate/sodium/potassium glasses doped with Sm3þ ions'', *Journal of Materials Research and Technology*, 47(4), 5587-5596, 2022.

[14] H. M. H. Zakaly, H. A. Saudi, S. A. M. Issa, M. Rashad, A. I. Elazaka, H. O. Tekin and Y. B. Saddeek, ''Alteration of optical, structural, mechanical durability and nuclear radiation attenuation

properties of barium borosilicate glasses through BaO reinforcement: experimental and numerical analyses'', *Ceramics International*, 47(2021), 5587-5596, 2021.

[15] H. Bircan , K. Manisa , A. S. Atan and M. Erdoğan , "Gama ve X-Işını Radyasyonu Yarı Değer Kalınlık Değerinin Hesaplanması için Yeni Bir Denklem", *Süleyman Demirel University Faculty of Arts and Science Journal of Science*, 12(1), 23-29, 2017.

[16] A. S. Ceyhan, ''Bazı metal elementlerinin ve biyolojik maddelerin 0,001-20 MeV enerji aralığında X-ışını radyasyonu kütle soğurma katsayılarının incelenmesi'', MS thesis, Department of Physics, Kutahya Dumlupınar University, Kutahya, Turkey 2018.

[17] J.H. Hubbell and S.M. Seltzer, 2004., Tables of X-Ray Mass Attenuation Coefficients and Mass EnergyAbsorption Coefficients (version 1.4). [Online]. National Institute of Standards and Technology, Gaithersburg, MD. Available: http://physics.nist.gov/xaamdi. Accessed: 17.04.2023.

[18] H. C. Manjunatha, L. Seenappa, K. N. Sridhar and C. Hanumantharayappa, ''Photon interaction parameters of different tissues of human organs'', *Defence Life Science Journal*, 2(3), 358-362, 2017.

[19] I. Jarrah, M. I. Radaideh, T. Kozlowski and Rizwan-Uddin, ''Determination and validation of photon energy absorption buildup factor in human tissues using Monte Carlo simulation'', *Radiation Physics and Chemistry*, 2019(160), 15-25, 2019.

[20] H. O. Tekin, G. Misned, S. A. M. Issa and H. M. H. Zakaly, ''A rapid and direct method for half value layer calculations for nuclear safety studies using MCNPX Monte Carlo code'', *Nuclear Engineering and Technology*, 54(9), 3317-3323, 2022.

Süleyman Demirel Üniversitesi Fen Edebiyat Fakültesi Fen Dergisi https://dergipark.org.tr/sdufeffd
Süleyman Demirel University Faculty of Arts and Sciences Journal of Science e-ISSN: 1306-7575
Research Article, 2023, 18(1): 18-27, DOI: 10.29233/sdufeffd.1266502

On the Jost Solutions of A Class of the Quadratic Pencil of the Sturm-Liouville Equation

Anar Adiloğlu Nabiev[1,*], Döndü Nurten Cücen[2]

[1]Computer Engineering Department, Faculty of Engineering, Suleyman Demirel University, 32260, Isparta, TURKEY
https://orcid.org/0000-0001-5602-5272
[2]Department of Mathematics, Art and Science Faculty, Suleyman Demirel University, 32260, Isparta, TURKEY
https://orcid.org/0000-0002-6032-9073
*corresponding author: anaradiloglu@sdu.edu.tr

(Received: 16.03.2023, Accepted: 25.04.2023, Published: 25.05.2023)

Abstract: In this study we construct new integral representations of Jost-type solutions of the quadratic pencil of the Sturm-Liouville equation with the piece-wise constant coefficient on the entire real line. Our aim is to express the special solutions of the Sturm-Liouville quadratic pencil in the form of some integral operators which kernels is related with the potential function of the Sturm-Liouville equation. This problem is technically diffucult due to the discontinous coefficient which causes the kernel function to also have a jump discontinuity.

Key words: Sturm-Liouville equation, operator pencil, transformation operator, diferantial equation with discontinuous cofficients, Jost solution

1. Introduction

We will focus at the Sturm-Liouville equation

$$-y'' + q(u)y + 2\tau p(u)y = \tau^2 \rho(u)y\,, u \in (-\infty, +\infty) \tag{1}$$

which has the discontinuous coefficient

$$\rho(u) = \begin{cases} 1, & u \geq 0 \\ \alpha^2, & u < 0 \end{cases} (\alpha \neq 1, \alpha > 0), \tag{2}$$

where $q(u)$ and $p(u)$ are real functions, τ is a complex parameter, $p(u)$ is absolutely continuous on every closed interval of the real axis and

$$\int_{-\infty}^{+\infty} |p(u)|du < \infty\,, \int_{-\infty}^{+\infty} (1+|u|)\left(|q(u)| + \left|p'(u)\right|\right)du < +\infty \tag{3}$$

Equation (1) arises when solving the Klein-Gordon equation with a static potential and zero charge in quantum scattering theory [7]. In addition, scattering problems arising in the theory of transmission lines, theories of electromagnetism, and the theory of elasticity are also reduced to equation (1). The transformation operators approach, which Marchenko [8,1] used to solve the inverse problems for the Sturm-Liouville

operator on a finite interval and on the half line, is an important method in inverse problems theory.

When $\rho(u) = 1$, there are enough studies in the literature for the direct and inverse problems of equation (1) [7, 6, 3, 11]. Inverse scattering problems related to the discontinuous Sturm-Liouville have been considered by many authors, for details we refer to [2, 9, 4, 5]. The direct and inverse scattering problems for equation (1) with $p(u) = 0$ in various settings have been investigated [4, 5, 13] where some integral representations, similar transformations operators for the Jost solutions (Js) of the Schroedinger equation, are obtained and applied for studying the discussed problems. In this study we construct new integral representations of Jost-type solutions of equation (1) on the entire axis under conditions (2) and (3). Our aim is to express the special solutions of the Sturm-Liouville quadratic pencil in the form of some integral operators which kernel is related with the potential of the equation (1). This problem is technically diffucult due to the discontinous coefficient which causes the kernel function to also have a jump discontinuity.

2. Integral representation of the Jost solutions

Let $g_{\pm}(u,\tau)$ are the solutions of (1) with the condition at infinity

$$\lim_{u\to\pm\infty} g_{\pm}(u,\tau)\exp\big(\mu i\tau(u)\big) = 1,$$

where $\exp(u) = e^{u}$ and $\mu(u) = u[\rho(u)]^{\frac{1}{2}}$. $g_{+}(u,\tau)$ and $g_{-}(u,\tau)$ are called the right and the left Jost solutions (rlJs) of (1) respectively. First, let's transform the given differential equation with the above conditions at infinity into an equivalent tintegral equation. We easily have

$$g_{\pm}(u,\tau) = F_{\pm}(u,\tau) + \int_{u}^{\pm\infty} N(u,t,\tau)\big(q(t) + 2\tau p(t)\big)g_{\pm}(t,\tau)dt \qquad (4)$$

where,

$$F_{+}(u,\tau) = F\left(u,\rho^{-\frac{1}{2}}(u),\tau\right) + F\left(u,-\rho^{-\frac{1}{2}}(u),-\tau\right)$$

$$F_{-}(u,\tau) = F\left(u,-\alpha\rho^{-\frac{1}{2}}(u),\tau\right) + F\left(u,\alpha\rho^{-\frac{1}{2}}(u),-\tau\right)$$

with

$$F(u,h(u),\tau) = \frac{1}{2}\big(1+h(u)\big)e^{i\tau\mu(u)}$$

and

$$N(u,t,\tau) = \frac{1}{2}\left(\rho^{-\frac{1}{2}}(t) - \rho^{-\frac{1}{2}}(u)\right)\int_{0}^{\mu(t)+\mu(u)} cos\tau s ds + \frac{1}{2}\left(\rho^{-\frac{1}{2}}(t) - \rho^{-\frac{1}{2}}(u)\right)\int_{0}^{\mu(t)-\mu(u)} cos\tau s ds$$

Think about the solution $g_+(u,\tau)$. It is known that [6, 3] for $u > 0$ and all $Im\tau \geq 0$ the solution $g_+(u,\tau)$ has the representation

$$g_+(u,\tau) = \exp(i\,\tau u + i\omega_+(u)) + \int_u^{+\infty} A^+(u,t)\exp(i\tau t)\,dt\,, \tag{5}$$

where $\omega_+(u) = \int_u^{+\infty} p(t)dt$ and the function $A^+(u,t)$ satisfies

$$\int_u^{+\infty} |A^+(u,t)| \leq C_0(exp(\sigma^+(u)) - 1) \tag{6}$$

for some constant $C_0 > 0$ and $\sigma^+(u) = \left(\int_u^{+\infty}(s-u)|q(t)| + 2|p(t)|\right)dt$. Furthermore, the kernel function $A^+(u,t)$ satisfies the condition

$$A^+(u,u) = \frac{1}{2}\left(\int_u^{+\infty}[q(t) + p^2(t)]dt - ip(u)\right)\exp\left(i\omega_+(u)\right). \tag{7}$$

For convenience afterwards we set $A^+(u,t) = F^+(w,z)$ with $w - z = u\,, w + z = t\,.$

Now we investigate the case $u < 0$ for the solution $g_+(u,\tau)$. Let us set $\alpha_\pm = \frac{1}{2}\left(1 \pm \frac{1}{\alpha}\right)$. In this case the equation (4) takes the form of

$$\begin{aligned} g_+(u,\tau) = {} & \alpha_+ \exp(i\alpha\tau u) + \alpha_- \exp(-i\alpha\tau u) \\ & - \int_u^0 \frac{sin\alpha\tau(u-s)}{\tau} q(s) g_+(s,\tau) ds \\ & + \int_0^\infty \left[\alpha^- \frac{sin\tau(\alpha u + s)}{\tau} - \alpha^+ \frac{sin\tau(\alpha u - s)}{\tau}\right] \\ & * [q(t) + 2\tau p(t)] g_+(s,\tau) ds \end{aligned} \tag{8}$$

We easily reveal that equation (8) has the solution

$$\begin{aligned} g_+(u,\tau) = {} & R_+(u)exp(i\alpha\tau u) + R_-(u)exp(-i\alpha\tau u) \\ & + \int_{\alpha u}^{+\infty} B^+(u,s)\exp(i\tau s)\,ds\,, Im\tau \geq 0, u < 0 \end{aligned} \tag{9}$$

where

$$R_\pm(u) = \alpha_\pm \exp(i\omega_+(0) \pm \frac{i}{\alpha}\int_u^0 p(\beta)d\beta)$$

and $B^+(u,s) = G^+(w,z)$ $(\alpha u = w - z\,, s = w + z)$ is defined after replacing $g_+(u,\tau)$ in equation (8) with formulas (5), (9) and transforming some integrals of the Fourier type:

$$G^+(w,z)=\frac{1}{2\alpha}\int_{\frac{w}{\alpha}}^{0} q(\beta)\,R_+(\beta)d\beta+\frac{1}{2\alpha}\int_{\frac{-z}{\alpha}}^{0} q(\beta)\,R_-(\beta)d\beta-\frac{i}{2\alpha^2}p\left(\frac{w}{\alpha}\right)R_+\left(\frac{w}{\alpha}\right)$$
$$+\frac{i}{2\alpha^2}p\left(\frac{-z}{\alpha}\right)R_-\left(\frac{-z}{\alpha}\right)+\frac{\alpha_+}{2}\int_0^{+\infty} q(\beta)e^{i\omega_+(\beta)}\,d\beta$$
$$-\frac{\alpha_-}{2}\int_0^{z} q(\beta)e^{i\omega_+(\beta)}\,d\beta-\frac{i\alpha_-}{2}p(z)e^{i\omega_+(z)}$$
$$+\alpha^+\int_0^{z}ds\int_s^{+\infty} q(\gamma-s)Z^+(\gamma,s)d\gamma-\alpha^-\int_0^{z}ds\int_s^{z} q(\gamma-s)Z^+(\gamma,s)d\gamma$$
$$+\frac{1}{\alpha^2}\int_0^{z}ds\int_w^{s} q\left(\frac{\gamma-s}{\alpha}\right)G^+(\gamma,s)d\gamma+i\alpha_+\int_z^{+\infty} p(\gamma-s)Z^+(\gamma,s)d\gamma$$
$$-i\alpha_-\int_0^{z} p(z-\delta)A^+(z,\delta)d\delta+\frac{1}{i\alpha^2}\int_0^{z} p\left(\frac{w}{\alpha}-\frac{\delta}{\alpha}\right)Z^+(w,\delta)d\delta$$
$$-\frac{1}{i\alpha^2}\int_w^{z} p\left(\frac{\gamma}{\alpha}-\frac{z}{\alpha}\right)G^+(\gamma,z)d\gamma\,,\qquad z>0\,,w<0$$

$$G^+(w,z)=\frac{\alpha^+}{2}\int_w^{+\infty} q(\beta)e^{i\omega_+(\beta)}\,d\beta+\frac{\alpha^-}{2}\int_z^{+\infty} q(\beta)e^{i\omega_+(\beta)}\,d\beta-\frac{i\alpha_-}{2}p(z)e^{i\omega_+(z)}$$
$$-\frac{i\alpha_+}{2}p(w)e^{i\omega_+(w)}+\alpha^+\int_w^{z}ds\int_\delta^{+\infty} q(\gamma-s)Z^+(\gamma,s)d\gamma$$
$$+\alpha^+\int_0^{z}ds\int_w^{+\infty} q(\gamma-s)Z^+(\gamma,s)d\gamma+\alpha^-\int_0^{z}ds\int_z^{+\infty} q(\gamma-s)Z^+(\gamma,s)d\gamma$$
$$-\alpha^-\int_w^{z}ds\int_s^{z} q(\gamma-s)A^+(\gamma-s,\gamma+s)d\gamma$$
$$+\frac{1}{\alpha^2}\int_w^{z}ds\int_w^{s} q\left(\frac{\gamma-s}{\alpha}\right)G^+(\gamma,s)d\gamma+\ i\alpha_+\int_z^{+\infty} p(\gamma-z)Z^+(\gamma,z)d\gamma$$
$$-\ i\alpha_+\int_0^{w} p(w-\delta)Z^+(w,\delta)d\delta$$
$$-i\alpha_-\int_0^{w} p(z-\delta)Z^+(z,\delta)d\delta+i\alpha_-\int_w^{+\infty} p(\gamma-w)Z^+(\gamma,w)d\gamma \tag{10}$$
$$+\frac{1}{i\alpha^2}\int_w^{z} p\left(\frac{w}{\alpha}-\frac{s}{\alpha}\right)G^+(w,s)ds$$
$$-\frac{1}{i\alpha^2}\int_w^{z} p\left(\frac{\gamma}{\alpha}-\frac{z}{\alpha}\right)G^+(\gamma,z)d\gamma\,,0<w<z\,. \tag{11}$$

Here we assume $A^+(u,t)\equiv 0$ for $t<u$ and $B^+(u,t)\equiv 0$ for $t<\alpha u$.

Similarly, when we consider the solution $g_-(u,\tau)$, we get for $u<0$

$$g_-(u,\tau)=exp(-i\alpha\tau u+i\omega_-(u))+\int_{-\infty}^{\alpha u}A^-(u,t)\exp(-i\tau t)\,dt\,,Im\tau\geq 0\,, \qquad (12)$$

where $\omega_-(u)=\frac{1}{\alpha}\int_{-\infty}^{u}p(t)dt$ and the kernel function $A^-(u,s)=Z^-(w,z),u=w+z,s=\alpha(w-z)$ satisfies the integral equation

$$\begin{aligned}Z^-(w,z)=&\frac{1}{2\alpha}\int_{-\infty}^{w}q(s)ds+\frac{1}{2i\alpha^2}p(w)e^{i\omega_-(w)}+\int_{-\infty}^{w}d\gamma\int_{0}^{z}q(\gamma+s)Z^-(\gamma,s)ds\\&+\frac{1}{i\alpha}\int_{0}^{z}p(w+\delta)\,A^-(w,\delta)d\delta\\&-\frac{1}{i\alpha}\int_{-\infty}^{w}p(\gamma+z)\,A^-(\gamma,z)d\gamma,w<-z\leq 0\end{aligned} \qquad (13)$$

which implies

$$\int_{-\infty}^{\alpha u}|A^-(u,t)dt|\leq C_1(exp(\sigma^-(u))-1) \qquad (14)$$

for some constant $C_1>0$ and $\sigma^-(u)=\left(\int_{-\infty}^{u}(u-s)|q(t)|+\frac{2}{\alpha}|p(t)|\right)dt$. Here $A^-(u,t)\equiv 0$ for $t>\alpha u$. Moreover, the kernel function $A^-(u,t)$ satisfies the condition

$$A^-(u,\alpha u)=\frac{1}{2\alpha}\left(\int_{-\infty}^{u}\left[q(t)+\frac{1}{\alpha^2}p^2(t)\right]dt+\frac{1}{2i\alpha}p(u)\right)\exp\big(i\omega_-(u)\big). \qquad (15)$$

As in the case of the (rJs) we have for $u>0$

$$\begin{aligned}g_-(u,\tau)=&T_+(u)exp(i\tau u)+T_-(u)exp(-i\tau u)\\&+\int_{-\infty}^{U}B^-(u,t)\exp(-i\tau t)\,dt\,,Im\tau\geq 0,u>0\end{aligned} \qquad (16)$$

where

$$T_{\pm}(u)=\frac{1}{2}(1\mp\alpha)e^{i\omega_-(0)\mp i\int_0^u p(s)ds}$$

and $B^-(u,s)=G^-(w,z),u=w+z,s=w-z$ with

$$G^-(w,z)=\frac{\alpha^-}{2}\int_{\frac{-z}{\alpha}}^{0}q(\beta)\,e^{i\omega_-(\beta)}d\beta+\frac{\alpha^+}{2}\int_{-\infty}^{0}q(\beta)\,e^{i\omega_-(\beta)}d\beta+\frac{1}{2}\int_{0}^{w}q(\beta)\,T_+(\beta)d\beta$$
$$+\frac{1}{2}\int_{0}^{z}q(\beta)\,T_-(\beta)d\beta+\frac{i\alpha_-}{2\alpha}p\left(\frac{-z}{\alpha}\right)e^{i\omega_-\left(\frac{-z}{\alpha}\right)}-\frac{i}{2}p(w)T_-(w)$$
$$+\frac{i}{2}p(z)T_+(z)+\alpha\alpha^-\int_{0}^{\frac{z}{\alpha}}ds\int_{\frac{-z}{\alpha}}^{-s}q(\gamma+s)Z^-(\gamma,s)d\gamma$$
$$+\alpha\alpha^+\int_{0}^{\frac{z}{\alpha}}ds\int_{-\infty}^{-s}q(\gamma+s)Z^-(\gamma,s)d\gamma+\int_{0}^{z}ds\int_{-s}^{w}q(\gamma+s)G^-(\gamma,s)d\gamma$$
$$+i\alpha_-\int_{0}^{\frac{z}{\alpha}}p\left(\frac{-z}{\alpha}+\gamma\right)Z^-\left(\frac{-z}{\alpha},\gamma\right)d\gamma$$
$$+i\alpha_+\int_{-\infty}^{\frac{-z}{\alpha}}p\left(\gamma+\frac{z}{\alpha}\right)Z^-\left(\gamma,\frac{z}{\alpha}\right)d\gamma+i\int_{-z}^{w}p(\gamma+z)G^-(\gamma,z)d\gamma \tag{17}$$
$$-\,i\int_{0}^{z}p(w+s)G^-(w,s)ds\ ,w>0\ ,z>0$$

$$G^-(w,z)=\frac{\alpha^+}{2}\int_{-\infty}^{\frac{w}{\alpha}}q(\beta)\,e^{i\omega_-(\beta)}d\beta-\frac{\alpha^-}{2}\int_{-\infty}^{\frac{-z}{\alpha}}q(\beta)\,e^{i\omega_-(\beta)}d\beta$$
$$+\frac{i\alpha_-}{2\alpha}p(-\alpha^{-1}z)e^{i\omega_-(-\alpha^{-1}z)}-\frac{i\alpha_+}{2\alpha}p(\alpha^{-1}w)e^{i\omega_-(\alpha^{-1}w)}$$
$$+\alpha^-\alpha\int_{\frac{-w}{\alpha}}^{\frac{z}{\alpha}}ds\int_{\frac{-z}{\alpha}}^{-s}q(\gamma+s)Z^-(\gamma,s)d\gamma$$
$$-\alpha^-\alpha\int_{0}^{\frac{-w}{2}}ds\int_{-\infty}^{\frac{-z}{\alpha}}q(\gamma+s)Z^-(\gamma,s)d\gamma$$
$$+\alpha\alpha^+\int_{0}^{\frac{-w}{\alpha}}ds\int_{-\infty}^{\frac{w}{\alpha}}q(\gamma+s)Z^-(\gamma,s)d\gamma$$
$$+\alpha\alpha^+\int_{\frac{-w}{\alpha}}^{\frac{z}{\alpha}}ds\int_{-\infty}^{-s}q(\gamma+s)Z^-(\gamma,s)d\gamma+\int_{-w}^{z}ds\int_{-s}^{w}q(\gamma+s)G^-(\gamma,s)d\gamma$$

$$-i\alpha_- \int_{-\infty}^{\frac{w}{\alpha}} p\left(\gamma-\frac{w}{\alpha}\right) Z^-(\gamma,w)d\gamma + i\alpha_- \int_0^{\frac{z}{\alpha}} p\left(-\frac{z}{\alpha}+\delta\right) Z^-\left(-\frac{z}{\alpha},\delta\right) d\delta$$
$$+ i\alpha_+ \int_{-\infty}^{\frac{-z}{\alpha}} p\left(\gamma+\frac{z}{\alpha}\right) Z^-\left(\gamma,\frac{z}{\alpha}\right) d\gamma$$
$$-i\alpha_+ \int_0^{\frac{-w}{\alpha}} p\left(\frac{w}{\alpha}+\delta\right) Z^-\left(\frac{w}{\alpha},\delta\right) d\delta + i\int_{-z}^{w} p(\gamma+z)G^-(\gamma,z)d\gamma \quad (18)$$
$$- i\int_0^{-z} p(w-\delta)G^-(w,\delta)d\delta \ , -z \le w < 0$$

and $B^-(u,t) \equiv 0$ for $t > u$. Estimating (10), (11) and (17), (18) and for some $C > 0$, we easily achieve

$$\pm \int_{\alpha u}^{\pm\infty} |B^{\pm}(u,t)|dt \le C\{exp(\sigma^{\pm}(\alpha u)) - 1\} \quad (19)$$

As a result of setting $K^{\pm}(u,t) = \begin{cases} A^{\pm}(u,t) & , \pm u \ge 0 \\ B^{\pm}(u,t) & , \pm u < 0 \end{cases}$ and combining all of our results, we may derive the following theorems.

Theorem 1. *If (3) is satisfied and* $Im\tau \ge 0$ *then the (Js)* $g_+(u,\tau)$ *has the representation*

$$g_+(u,\tau) = R_+(u)e^{i\tau\mu(u)} + R_-(u)e^{i\tau\mu(u)} + \int_{\mu(u)}^{+\infty} K^+(u,t)\, e^{i\tau t}dt\,, \quad (20)$$

where,

$$R_+(u) = \frac{1}{2}\left(1+\left(\rho(u)\right)^{-\frac{1}{2}}\right) exp\left(\int_u^{+\infty} i\left(\rho(t)\right)^{-\frac{1}{2}} p(t)dt\right),$$
$$R_-(u) = \frac{1}{2}\left(1-\left(\rho(u)\right)^{-\frac{1}{2}}\right) exp\left(i\int_u^{+\infty} \left(\rho(t)\right)^{-\frac{1}{2}} p(t)sgntdt\right),$$

$\mu(u) = u[\rho(u)]^{-\frac{1}{2}}$ *and* $K^+(u,t)$ *satisfies*

$$\int_{\mu(u)}^{+\infty} |K^+(u,t)|dt \le C\{exp(\sigma^+(u)) - 1\} \ (C > 0). \quad (21)$$

Furthermore,

$$K^{+}\big(u,\mu(u)\big)=R_{+}(u)\left\{\frac{1}{2}\int_{u}^{+\infty}\Big(\rho^{-\frac{1}{2}}(s)q(s)+\rho^{-\frac{3}{2}}(s)p^{2}(s)\Big)\,ds+\frac{i}{2}\int_{u}^{+\infty}\left[\left(\frac{1}{\rho^{\frac{1}{2}}(s)}\right)^{2}+\left(1-\frac{\rho^{\frac{1}{2}}(s)}{\rho^{\frac{1}{2}}(x)}\right)^{2}\right]p'(s)ds\right\},\tag{22}$$

$$K^{+}(u,t)\big|_{t=-\mu(u)-0}^{t=-\mu(u)+0}=R_{-}(u)\left\{\frac{1}{2}\int_{u}^{+\infty}\Big(\rho^{-\frac{1}{2}}(s)q(s)+\rho^{-\frac{3}{2}}(s)p^{2}(s)\Big)\,sgns\,ds+\frac{i}{2}\int_{u}^{+\infty}\left[\left(\frac{1}{\rho^{\frac{1}{2}}(s)}\right)^{2}+\left(1+\frac{(sgns)\rho^{\frac{1}{2}}(s)}{\rho^{\frac{1}{2}}(x)}\right)^{2}\right]p'(s)ds\right\},\tag{23}$$

where $sgn\ s$ is the sign function.

Theorem 2. *If (3) is satisfied and $Im\tau\geq 0$ then the (Js) $g_{-}(u,\tau)$ of equation (1) has the representation*

$$g_{-}(u,\tau)=T_{+}(u)e^{i\tau\mu(u)}+T_{-}(u)e^{i\tau\mu(u)}+\int_{-\infty}^{\mu(u)}K^{-}(u,t)\,\mathrm{e}^{-\mathrm{i}\tau\mathrm{t}}dt\,,\tag{24}$$

where,

$$T_{+}(u)=\frac{1}{2}\Big(1-\alpha\big(\rho(u)\big)^{-\frac{1}{2}}\Big)exp\left(\int_{-\infty}^{u}-i\rho(t)^{-\frac{1}{2}}\,p(t)\,sgntdt\right),$$

$$T_{-}(u)=\frac{1}{2}\Big(1+\alpha\big(\rho(u)\big)^{-\frac{1}{2}}\Big)exp\left(\int_{-\infty}^{u}i\rho(t)^{-\frac{1}{2}}\,p(t)\,dt\right),$$

$\mu(u)=u[\rho(u)]^{\frac{1}{2}}$ and $K^{-}(u,t)$ satisfies the inequality

$$\int_{-\infty}^{\mu(u)}|K^{-}(u,t)|dt\leq C\{exp(\sigma^{-}(u))-1\}\ (C>0)\,.\tag{25}$$

Furthermore, the following expressions are fulfilled:

$$K^{-}\big(u,\mu(u)\big)=T_{-}(u)\left\{\frac{1}{2}\int_{-\infty}^{u}\Big(\rho^{-\frac{1}{2}}(s)q(s)+\rho^{-\frac{3}{2}}(s)p^{2}(s)\Big)\,ds-\frac{i}{2}\int_{-\infty}^{u}\left[\left(\frac{1}{\rho^{\frac{1}{2}}(s)}\right)^{2}+\left(1-\frac{\rho^{\frac{1}{2}}(x)}{\rho^{\frac{1}{2}}(s)}\right)^{2}\right]p'(s)ds\right\},\tag{26}$$

$$K^{-}(u,t)\Big|_{t=-\mu(u)-0}^{t=-\mu(u)+0} = T_{+}(u)\left\{\frac{1}{2}\int_{-\infty}^{U}\left(\rho^{-\frac{1}{2}}(s)q(s)+\rho^{-\frac{3}{2}}(s)p^{2}(s)\right)sgnsds + \frac{i}{2}\int_{-\infty}^{u}\left[1+\left(1-\frac{(sgns)\rho^{\frac{1}{2}}(s)}{\rho^{\frac{1}{2}}(x)}\right)^{2}\right]p'(s)ds\right\}, \quad (27)$$

where sgns is the sign function.

4. Conclusion

In this paper, new integral representations for the quadratic pencil of Sturm-Liouville equation with discontinuous coefficients are obtained and, with their help, a connection is established between the potential functions of the equation and the kernel in the representation of the solution. This result is important in studying the properties of spectral data and in solving the inverse scattering problem.

Authorship contribution statement

A. N. Adiloğlu: Conceptualization, Methodology, Supervision.

N. D. Cücen: Data Curation, Original Draft Writing.

Declaration of competing interest

The authors declare that they have no known competing financial interests or personal relationships that could have appeared to influence the work reported in this paper.

Ethics Committee Approval and/or Informed Consent Information

As the authors of this study, we declare that we do not have any ethics committee approval and/or informed consent statement.

References

[1] B. M. Levitan and M. G. Gasymov, "Determination of a differential equation by two spectra", *Uspehi Mat. Nauk*, 19(2), 3-63, 1964.

[2] M. G. Gasymov, "The direct and inverse problem of spectral analysis for a class of equations with a discontinuous coefficient", in Non- classical methods in geophysics, Editors: M. M. Lavrent'ev. Novosibirsk Nauka, 1977, 37-44 (in Russian).

[3] F. G. Maksudov and G. Sh. Guseinov, "On the solution of the inverse scattering problem for the quadratic pencil of the Schrödinger equation on the full-line", *Dokl. Akad. Nauk USSR*, 289(1), 42-46, 1986.

[4] H. M. Huseynov and J. A. Osmanl, "Inverse scattering problem for one-dimensional Schrö dinger equation with discontinuity conditions", *Journal of Mathematical Physics, Analysis, Geometry*, 9(3), 332-359, 2013.

[5] A. A. Nabiev and Kh. R. Mamedov, "On the Jost solutions for a class of Schrödinger equations with piecewise constant coefficients", *Journal of Mathematical Physics, Analysis, Geometry*, 11, 279-296, 2015.

[6] M. Jaulent and C. Jean, "The inverse problem for the one dimensional Schrödinger equation with an energy dependent potential, I, II", *Ann. Inst. Henri Poincare*, 25, 105-118, 1976.

[7] D. J. Kaup, "A higher-order water-wave equation and the method for solving it", *Prog. Theor. Phys.*, 54, 396-408, 1975.

[8] V. A. Marchenko, Sturm-Liouville Operators and Their Applications, Basel: Birkhauser, 1986.

[9] Kh. R. Mamedov, "On an inverse scattering problem for a discontinuous Sturm-Liouville equation with a spectral parameter in the boundary condition", *Boundary Value Problems*, Article ID 171967, 17 pages, 2010.

[10] Kh. R. Mamedov and A. A. Nabiev, “Inverse problem of scattering theory for a class one-dimensional Schrö dinger equation”, *Quastiones Math.*, 42(7), 841-856, 2019.
[11] Y. Kamimura, “An inversion formula in energy dependent scattering”, *Journal of Integral Equations and Applications*, 19(4), 473-512, 2007.
[12] K. Chadan and P. C. Sabatier, Inverse Problems in Quantum Scattering Theory, Springer, New York, 1989.
[13] A. A. Nabiev, “Direct and inverse scattering problem for the one dimensional Schrödinger equation with energy dependent potential and discontinuity conditions”, *Proceedings of the Institute of Mathematics and Mechanics National Academy of Sciences of Azerbaijan*, 40, 315-331, 2014.